ELSEVIER

Fluid Dynamics Research 28 (2001) 397–421

FLUID DYNAMICS RESEARCH

Turbulent penetrative convection with an internal heat source

J.R. Chasnov*, K.L. Tse [1]

Department of Mathematics, The Hong Kong University of Science and Technology, Clear Water Bay, Kowloon, Hong Kong

Received 14 October 2000; accepted 18 December 2000

Abstract

An infinite fluid with a vertical cubic temperature profile in the absence of fluid motion is considered as a model for penetrative convection in which a central unstably stratified fluid layer is bounded above and below by stably stratified layers. Turbulence statistics from direct and large eddy numerical simulations for the mean temperature gradient, the velocity and temperature variances and the heat flux are presented for Rayleigh numbers R up to four orders of magnitude above critical. By means of a simplified second-moment closure, analytical scaling laws for the statistics are determined. For high Rayleigh numbers, the mean temperature gradient approaches zero in a central well-mixed layer, a reduced positive (stable) value in upper and lower partially mixed layers, and an unmixed value far above and below. The temperature variance is a factor of $R^{1/3}$ larger in the partially mixed layers compared to the well-mixed layer; the velocity variance and heat flux scales the same in both layers. Approximation of the three layers by a two layer model yields an estimate for the height of the mixed layer: the height decreases slowly with increasing Rayleigh number and at the highest Rayleigh number simulated is approximately 30% longer than the unstable layer in the absence of fluid motion.

PACS: 47.27.-i; 47.27.Eq

Keywords: Penetrative convection; Turbulence; Mixing; Numerical simulation; Turbulence modelling

1. Introduction

Penetrative convection occurs when vertical buoyancy-driven motion originating in an unstably stratified layer of fluid penetrates into surrounding stably stratified layers. If the Reynolds number of the flow field is sufficiently large, the fluid motion will be turbulent. A review of penetrative convection with many references to previous work in the field can be found in the monograph of Straughan (1993).

There are several well-known physical examples of penetrative convection. A laboratory experiment can be realized using an insulated container of water with a bottom ice surface fixed at

* Corresponding author.
E-mail address: jeffrey.chasnov@ust.hk (J.R. Chasnov).
[1] Present address: Department of Mathematics, Arizona State University, Tempe, AZ 85287, USA.

0169-5983/01/$20.00
PII: S0169-5983(00)00037-X

temperature 0°C and a top air surface at temperature 25°C, say (Townsend, 1964). The maximum density of water at 4°C makes the bottom layer gravitationally unstable and convective motion generated there will penetrate into the stable layer above. Penetrative convection is also common in the environment. On a sunny morning, the nocturnal inversion is replaced by a growing unstable layer adjacent to the warming ground. Surface cooling of sea water by evaporation can result in a gravitationally unstable surface layer which is transported downwards into the lower stably stratified layers. Penetrative convection also occurs in stars (Canuto and Christensen-Dalsgaard, 1998). Stars with mass less than approximately one solar mass have a radiative core and a convective envelope; more massive stars have a convective core and a radiative envelope. Turbulent motion in the convective zone may penetrate into the stably stratified radiative zones. The amount of materials being mixed due to penetrative convection is a crucial ingredient in stellar evolution theories and is an important topic of interest to astrophysicists.

Due to its geophysical and astrophysical importance, there have been many studies of penetrative convection, both in the laboratory and using mathematical models with varying degrees of complexity. Our interest here is in *turbulent* penetrative convection, and to perform relatively high Reynolds number simulations we adopt a simple mathematical model proposed by Matthews (1988). This model of penetrative convection within the Boussinesq approximation uses a cubic temperature profile, maintained by internal heating. Matthews studied the linear stability of such a temperature profile, computed the critical Rayleigh number R_c, and showed that the low Rayleigh number bifurcation to convective motion is supercritical with rolls preferred to squares. Here we consider the corresponding high Rayleigh number problem, corresponding to high Reynolds numbers, for which the convective motion is turbulent. Our methods of enquiry will be three-dimensional direct numerical simulation (DNS) of the flow field up to Rayleigh numbers of about $10^2 R_c$ and large eddy simulation (LES) up to Rayleigh numbers of $10^4 R_c$. A simplified second-moment closure turbulence model will be used to predict the asymptotic scaling of the statistics with Rayleigh number.

Although we adopt the mathematical model of Matthews, our work is closer in spirit to that of Zahn et al. (1982). The Zahn et al. mathematical model is also of simple form, and is equivalent to replacing the Matthews cubic temperature profile by a piecewise linear profile, with an unstable temperature gradient bounded above and below by stable temperature gradients. We note that the linear stability of such a profile was considered much earlier by Gribov and Gurevich (1957). Zahn et al. considered numerical solutions of their equations up to 10^5 times critical. However, solutions were obtained using one or two mode planform functions to represent the horizontal motion, and so contain some arbitrariness based on the choice of planform functions. Nevertheless, much interesting physics was uncovered by their work.

2. Formulation of the problem

Herein, the vertical coordinate is denoted by x_2. Let $T(\boldsymbol{x}, t)$ be the temperature of a fluid at position $\boldsymbol{x}$ and time t. We decompose T as

$$T(\boldsymbol{x}, t) = T_0(x_2) + \theta(\boldsymbol{x}, t), \tag{1}$$

where $T_0(x_2)$ is the vertical variation of the temperature field in the absence of fluid motion, and $\theta(\boldsymbol{x}, t)$ is the change in T induced by the fluid motion. The variation $T_0(x_2)$ satisfies the heat

conduction equation

$$\kappa \frac{\mathrm{d}^2}{\mathrm{d}x_2^2} T_0 = -Q, \tag{2}$$

where κ is the thermal conductivity and $Q(x_2)$ represents a steady internal heat source assumed herein to be unaffected by the fluid motion. With this definition, the governing equations for the velocity and temperature field of the fluid may be written within the well-known Boussinesq approximation as (Spiegel and Veronis, 1960)

$$\frac{\partial}{\partial t}\boldsymbol{u} + \boldsymbol{u}\cdot\nabla\boldsymbol{u} = -\nabla p + \boldsymbol{x}_2 g\alpha\theta + \nu\nabla^2\boldsymbol{u}, \tag{3}$$

$$\frac{\partial}{\partial t}\theta + \boldsymbol{u}\cdot\nabla\theta = u_2\beta_0 + \kappa\nabla^2\theta, \tag{4}$$

$$\nabla\cdot\boldsymbol{u} = 0, \tag{5}$$

where $\boldsymbol{u}$ is the fluid velocity, p a pressure-like term which serves to enforce continuity, $g > 0$ the gravitational acceleration with $\boldsymbol{x}_2$ the unit vector in the vertical direction, α the coefficient of thermal expansion and ν the kinematic viscosity. Finally,

$$\beta_0(x_2) = -\left(\frac{\mathrm{d}T_0}{\mathrm{d}x_2} + \frac{g}{C_p}\right) \tag{6}$$

is the vertical superadiabatic gradient of the temperature in the quiescent fluid, where C_p is the specific heat at constant pressure. The problem of penetrative convection in an infinite domain in the present formulation, for which the turbulent motion in horizontal planes may be considered homogeneous, requires only specification of $\beta_0(x_2)$. If it is desired to have an unstable layer of fluid bounded above and below by stable layers, then β_0 must be positive in some central region, and negative in regions above and below this central core. Matthews (1988) chooses the simple form

$$\beta_0(x_2) = B - 3Ax_2^2 \tag{7}$$

with A and B positive constants. Zahn et al. (1982), following Gribov and Gurevich (1957), choose the piecewise constant form

$$\beta_0(x_2) = \begin{cases} \beta_\mathrm{u} & \text{if } |x_2| < d/2, \\ \beta_\mathrm{s} & \text{if } |x_2| > d/2, \end{cases} \tag{8}$$

where $\beta_\mathrm{u} > 0$ and $\beta_\mathrm{s} < 0$ are fixed constants. The ratio $|\beta_\mathrm{s}|/\beta_\mathrm{u}$ introduces an additional nondimensional group in their formulation.

Although the mathematical problem of penetrative convection defined above is well-posed after choosing β_0, its physical interpretation may differ. Matthews considers the adiabatic temperature gradient g/C_p to be negligible and the temperature gradient $\mathrm{d}T_0/\mathrm{d}x_2$ to be due to a steady internal heat source $Q(x_2) = -6\kappa A x_2$. Zahn et al. consider a constant radiative temperature gradient $\mathrm{d}T_0/\mathrm{d}x_2$ and an adiabatic gradient g/C_p which varies piecewise constant to yield their desired form of β_0, given by Eq. (8). Herein for convenience, we will adopt both the Matthews form for β_0 as well as

his physical point of view. The temperature variation in the absence of motion then takes the cubic form

$$T_0(x_2) = Ax_2^3 - Bx_2, \tag{9}$$

where we have adjusted the temperature scale to be zero at $x_2 = 0$.

Nondimensionalization of our variables requires a length, time and temperature scale. The length scale may be chosen as $d = \sqrt{B/A}$ and the temperature scale as Bd. Both Matthews and Zahn et al. choose d^2/κ as the time scale. However, another possible choice is $1/\sqrt{g\alpha B}$, and this may be more natural at high Rayleigh numbers when thermal mixing is mainly due to turbulent rather than molecular conductivity. With this latter choice of time scale, the nondimensional form of Eqs. (3)–(5) is

$$\frac{\partial}{\partial t}\boldsymbol{u} + \boldsymbol{u}\cdot\nabla\boldsymbol{u} = -\nabla p + \boldsymbol{x}_2\theta + \sqrt{\frac{\sigma}{R}}\nabla^2\boldsymbol{u}, \tag{10}$$

$$\frac{\partial}{\partial t}\theta + \boldsymbol{u}\cdot\nabla\theta = u_2\beta_0 + \frac{1}{\sqrt{\sigma R}}\nabla^2\theta, \tag{11}$$

$$\nabla\cdot\boldsymbol{u} = 0, \tag{12}$$

where the nondimensional superadiabatic temperature gradient is given by

$$\beta_0(x_2) = 1 - 3x_2^2 \tag{13}$$

and the two nondimensional groups of our problem, the Rayleigh number R and the Prandtl number σ, are given by

$$R = \frac{g\alpha B d^4}{\nu\kappa}, \quad \sigma = \frac{\nu}{\kappa}. \tag{14}$$

For later comparison with the results of Zahn et al., we note that the above equations may be transformed into a normalization using the diffusion time scale in place of the buoyancy time scale by the following replacements:

$$\boldsymbol{u} \to \boldsymbol{u}/\sqrt{\sigma R}, \quad t \to t\sqrt{\sigma R} \tag{15}$$

the normalization of p is arbitrary because of the incompressibility condition (12).

The main goal of our work is to determine the turbulent statistically steady-state solutions of Eqs. (10)–(12) as a function of the nondimensional groups of our problem. For simplicity, we consider only the region of parameter space for which both the turbulent viscosity and turbulent conductivity are much larger than their molecular counterparts; i.e., both σR and R/σ are large. The interesting physics associated with this problem may be explored by considering $\sigma = 1$ and $R \gg 1$. Direct numerical simulations (DNS) and large eddy simulations (LES) can be performed over several orders of magnitude of R above its critical value, determined by Matthews (1988) to be $R_c = 88.0$.

Our main interest is in the first- and second-moments of the velocity and temperature fields. In particular, we are interested in elucidating the asymptotic behavior of these statistics at large R. Statistical averages denoted by $\langle\ldots\rangle$ may be performed over independent realizations of the fields, or equivalently by spatial averages in horizontal planes together with time averages taken in the statistically steady state. All resulting statistics will be functions only of the vertical coordinate x_2.

The only nonzero first-moments are the average temperature and pressure, the mean velocity being zero, and we decompose the temperature $\theta(\boldsymbol{x},t)$ and pressure $p(\boldsymbol{x},t)$ into mean and fluctuating components:

$$\theta = \langle\theta\rangle + \theta', \quad p = \langle p\rangle + p'. \tag{16}$$

The only independent second-moments are $\langle u_2^2\rangle$, $\langle u_1^2+u_3^2\rangle$, $\langle u_2\theta'\rangle$, and $\langle\theta'^2\rangle$, all other second-moments being zero or trivially related due to the statistical isotropy in horizontal planes.

At this point, it is worthwhile to note the up-down symmetry of governing equations (10)–(12). Since our choice of superadiabatic temperature gradient β_0 is symmetric in x_2, i.e., $\beta_0(-x_2)=\beta_0(x_2)$, the governing equations are seen to be invariant under the transformation

$$x_2 \to -x_2, \quad u_2 \to -u_2, \quad \theta \to -\theta.$$

It is expected that the moments will also obey this same symmetry, so that the second-moments $\langle u_2^2\rangle, \langle u_1^2+u_3^2\rangle, \langle\theta'^2\rangle$ and $\langle u_2\theta'\rangle$ will be symmetric about the origin, whereas $\langle\theta\rangle$ will be antisymmetric.

Our interest is in turbulent flow, which usually implies large Reynolds numbers $Re = UL/\nu$, where U and L are characteristic velocity and length scales of the flow field, respectively. We can take U equal to the velocity variance at $x_2 = 0$, and $L = d$, where d is the length scale used in the nondimensionalization of our equations. With U and L made nondimensional, the Reynolds number Re is related to the Raleigh number R by

$$Re = U\sqrt{\frac{R}{\sigma}}, \tag{17}$$

where the nondimensional velocity U is as yet an unknown function of R, although it is expected that Re will increase with R.

3. Equations for the statistics

To gain some preliminary insight into our problem, it is worthwhile to first construct equations for the first- and second-moments. We work from the nondimensional governing equations (10)–(12).

3.1. First-moments

We begin by considering the statistical average of the velocity and temperature equations. First, taking the statistical average of the temperature equation (11) and integrating from $-\infty$ to x_2 with boundary condition u_2 and $\mathrm{d}\langle\theta\rangle/\mathrm{d}x_2$ vanishing at infinity, we obtain

$$\frac{\mathrm{d}}{\mathrm{d}x_2}\langle\theta\rangle = \sqrt{\sigma R}\langle u_2\theta'\rangle. \tag{18}$$

The heat flux $\langle u_2\theta'\rangle$ is thus simply related to the change in the mean temperature gradient induced by the fluid motion. Integrating (18) over the vertical domain, and using the antisymmetry of $\langle\theta\rangle$, we see that as a consequence of convection the temperature of the fluid is raised far above the convectively unstable layer (or lowered far below) by a constant given by

$$\theta_\infty = \frac{1}{2}\sqrt{\sigma R}\int_{-\infty}^{\infty}\langle u_2\theta'\rangle\,\mathrm{d}x_2. \tag{19}$$

We will see later by means of the second-moment equations that this constant is directly related to the dissipation of kinetic energy by the turbulence.

Now, taking the statistical average of the velocity equation (10), we obtain

$$\frac{\mathrm{d}}{\mathrm{d}x_2}(\langle u_2^2\rangle + \langle p\rangle) = \langle\theta\rangle, \tag{20}$$

which can be used to eliminate $\langle p\rangle$ from the equations for the second-moments.

3.2. Second-moments

The budget equations for the second-moments are well known (Launder, 1989). Although the time-derivative terms are identically zero in a statistically steady state, we include them for clarity. The budget equations for the vertical and horizontal velocity variances $\langle u_2^2\rangle$ and $\langle u_1^2 + u_3^3\rangle$ are given by

$$\frac{\partial}{\partial t}\langle u_2^2\rangle = \mathrm{I}_{\langle u_2^2\rangle} + \mathrm{II}_{\langle u_2^2\rangle} + \mathrm{III}_{\langle u_2^2\rangle} + \mathrm{IV}_{\langle u_2^2\rangle}, \tag{21}$$

where

$$\mathrm{I}_{\langle u_2^2\rangle} = -2\sqrt{\frac{\sigma}{R}}\left\langle \frac{\partial u_2}{\partial x_j}\frac{\partial u_2}{\partial x_j}\right\rangle,$$

$$\mathrm{II}_{\langle u_2^2\rangle} = \frac{\partial}{\partial x_2}\left(\sqrt{\frac{\sigma}{R}}\frac{\partial}{\partial x_2}\langle u_2^2\rangle - \langle u_2^3\rangle - 2\langle u_2 p'\rangle\right),$$

$$\mathrm{III}_{\langle u_2^2\rangle} = 2\left\langle p'\frac{\partial u_2}{\partial x_2}\right\rangle,$$

$$\mathrm{IV}_{\langle u_2^2\rangle} = 2\langle u_2\theta'\rangle$$

and

$$\frac{\partial}{\partial t}\langle u_1^2 + u_3^2\rangle = \mathrm{I}_{\langle u_1^2+u_3^2\rangle} + \mathrm{II}_{\langle u_1^2+u_3^2\rangle} + \mathrm{III}_{\langle u_1^2+u_3^2\rangle}, \tag{22}$$

where

$$\mathrm{I}_{\langle u_1^2+u_3^2\rangle} = -2\sqrt{\frac{\sigma}{R}}\left\langle \frac{\partial u_1}{\partial x_j}\frac{\partial u_1}{\partial x_j} + \frac{\partial u_3}{\partial x_j}\frac{\partial u_3}{\partial x_j}\right\rangle,$$

$$\mathrm{II}_{\langle u_1^2+u_3^2\rangle} = \frac{\partial}{\partial x_2}\left(\sqrt{\frac{\sigma}{R}}\frac{\partial}{\partial x_2}\langle u_1^2 + u_3^2\rangle - \langle u_2(u_1^2 + u_3^2)\rangle\right),$$

$$\mathrm{III}_{\langle u_1^2+u_3^2\rangle} = 2\left\langle p'\frac{\partial u_1}{\partial x_1} + p'\frac{\partial u_3}{\partial x_3}\right\rangle.$$

For later use, we also write the equation for the total velocity variance $q^2 = \langle u_2^2\rangle + \langle u_1^2 + u_3^2\rangle$, determined by summing the two equations above. The pressure-strain terms denoted by III cancel because of the

continuity equation (12), serving only the purpose of moving energy among the velocity components, and we find

$$\frac{\partial}{\partial t}q^2 = \mathrm{I}_{q^2} + \mathrm{II}_{q^2} + \mathrm{IV}_{q^2}, \tag{23}$$

where

$$\mathrm{I}_{q^2} = -2\sqrt{\frac{\sigma}{R}}\left\langle \frac{\partial u_i}{\partial x_j}\frac{\partial u_i}{\partial x_j}\right\rangle,$$

$$\mathrm{II}_{q^2} = \frac{\partial}{\partial x_2}\left(\sqrt{\frac{\sigma}{R}}\frac{\partial}{\partial x_2}q^2 - \langle u_2 q^2\rangle - 2\langle u_2 p'\rangle\right),$$

$$\mathrm{IV}_{q^2} = 2\langle u_2\theta'\rangle.$$

The budget equations for the temperature variance and the heat flux are given by

$$\frac{\partial}{\partial t}\langle\theta'^2\rangle = \mathrm{I}_{\langle\theta'^2\rangle} + \mathrm{II}_{\langle\theta'^2\rangle} + \mathrm{IV}_{\langle\theta'^2\rangle}, \tag{24}$$

where

$$\mathrm{I}_{\langle\theta'^2\rangle} = -\frac{2}{\sqrt{\sigma R}}\left\langle \frac{\partial\theta'}{\partial x_j}\frac{\partial\theta'}{\partial x_j}\right\rangle,$$

$$\mathrm{II}_{\langle\theta'^2\rangle} = \frac{\partial}{\partial x_2}\left(\frac{1}{\sqrt{\sigma R}}\frac{\partial}{\partial x_2}\langle\theta'^2\rangle - \langle u_2\theta'^2\rangle\right),$$

$$\mathrm{IV}_{\langle\theta'^2\rangle} = -2\langle u_2\theta'\rangle\frac{\partial\langle T\rangle}{\partial x_2}$$

and

$$\frac{\partial}{\partial t}\langle u_2\theta'\rangle = \mathrm{I}_{\langle u_2\theta'\rangle} + \mathrm{II}_{\langle u_2\theta'\rangle} + \mathrm{III}_{\langle u_2\theta'\rangle} + \mathrm{IV}_{\langle u_2\theta'\rangle}, \tag{25}$$

where

$$\mathrm{I}_{\langle u_2\theta'\rangle} = -\left(\sqrt{\frac{\sigma}{R}} + \frac{1}{\sqrt{\sigma R}}\right)\left\langle \frac{\partial\theta'}{\partial x_j}\frac{\partial u_2}{\partial x_j}\right\rangle,$$

$$\mathrm{II}_{\langle u_2\theta'\rangle} = \frac{\partial}{\partial x_2}\left(\sqrt{\frac{\sigma}{R}}\left\langle\theta'\frac{\partial u_2}{\partial x_2}\right\rangle + \frac{1}{\sqrt{\sigma R}}\left\langle u_2\frac{\partial\theta'}{\partial x_2}\right\rangle - \langle u_2^2\theta'\rangle\right),$$

$$\mathrm{III}_{\langle u_2\theta'\rangle} = -\left\langle\frac{\partial p'}{\partial x_2}\theta'\right\rangle,$$

$$\mathrm{IV}_{\langle u_2\theta'\rangle} = \langle\theta'^2\rangle - \langle u_2^2\rangle\frac{\partial\langle T\rangle}{\partial x_2}.$$

The mean temperature gradient $\partial\langle T\rangle/\partial x_2$ is given in terms of the heat flux $\langle u_2\theta'\rangle$ using Eqs. (1), (6) (with $C_p \to \infty$), and Eq. (18) by

$$\frac{\partial\langle T\rangle}{\partial x_2} = \sqrt{\sigma R}\langle u_2\theta'\rangle - \beta_0. \tag{26}$$

The description of the terms in the budget equations are standard: terms denoted by I represent viscous and/or conductive dissipation; by II transport along the inhomogeneous vertical direction; by III pressure redistribution, and; by IV source or sink terms due to buoyancy and/or stratification.

An important relation can be derived from the budget equation for q^2 after integrating over the vertical direction so that the contribution from the transport term II_{q^2} vanishes. If we define the (nondimensional) vertically integrated horizontally averaged energy $(q^2/2)$ dissipation per unit mass as

$$\varepsilon = \sqrt{\frac{\sigma}{R}} \int_{-\infty}^{\infty} \left\langle \frac{\partial u_i}{\partial x_j} \frac{\partial u_i}{\partial x_j} \right\rangle \mathrm{d}x_2 \tag{27}$$

then using Eq. (19), we derive

$$\theta_\infty = \frac{1}{2}(\sigma R)^{1/2} \varepsilon. \tag{28}$$

The rise in the temperature of the fluid (given by θ_∞) far above the unstable layer (or the decrease in temperature far below) is thus seen to be directly proportional to the vertically integrated energy dissipation ε.

An additional relation may be obtained upon vertical integration of the temperature variance budget equation (24). If we define the vertically integrated horizontally averaged (one-half) temperature variance dissipation per unit mass as

$$\varepsilon_\theta = \frac{1}{\sqrt{\sigma R}} \int_{-\infty}^{\infty} \left\langle \left(\frac{\partial \theta'}{\partial x_j} \right)^2 \right\rangle \mathrm{d}x_2 \tag{29}$$

then we derive the relation

$$\varepsilon_\theta = -\int_{-\infty}^{\infty} \langle u_2 \theta' \rangle \frac{\partial \langle T \rangle}{\partial x_2} \mathrm{d}x_2 \tag{30}$$

which by the use of Eq. (26) relates the temperature variance dissipation rate to an integral over the heat flux. The heat flux thus determines both the integrated velocity and temperature variance dissipation rates.

4. Numerical simulation methodology

Periodic boundary conditions are used in the two horizontal directions for which the turbulence is homogeneous. A pseudospectral method was implemented on a parallel computer. In the periodic directions complex exponentials are used as basis functions; in the inhomogeneous direction, either Hermite basis functions (Tse and Chasnov, 1998) or Chebychev polynomials with an algebraic map which transforms the infinite vertical domain to a finite interval (Tse, 2000) are used. Although both methods yield essentially the same results, the Chebychev approach proved to be more efficient. Details of these numerical methods may be found in the above citations.

The computations are performed in nondimensional units (see Section 2) and in these units the periodicity length in the horizontal direction is 20.944; this approximates well an infinite horizontal extent. In the vertical direction, the outermost collocation points are separated by a distance of 6 using Hermite functions, and 35.8 using Chebychev polynomials, though the internal spacing of the

points are different with these methods so that these numbers cannot be compared. A grid resolution of 64 points in each direction enabled us to perform direct numerical simulations (DNS) up to a Rayleigh number of 10^4. For Rayleigh numbers 10^5 and 10^6, the resolution was increased to 128 points in each direction and subgrid scale stress terms in standard form were added to the right-hand sides of the momentum and temperature equations, (10) and (11), respectively

$$-\frac{\partial \tau_{ij}}{\partial x_j}, \quad -\frac{\partial \tau_j^\theta}{\partial x_j},$$

where τ_{ij} and τ_j^θ are modelled as (Smagorinsky, 1963)

$$\tau_{ij} = -\frac{(C\Delta)^2}{\sqrt{2}} S S_{ij} + \frac{1}{3}\tau_{kk}\delta_{ij}, \tag{31}$$

$$\tau_j^\theta = -\frac{(C\Delta)^2}{\sqrt{2}\sigma_e} S \frac{\partial \theta}{\partial x_j} \tag{32}$$

with $S_{ij} = (\partial u_i/\partial x_j + \partial u_j/\partial x_i)$, $S = \sqrt{S_{ij}S_{ij}}$, Δ the horizontal grid spacing, σ_e an eddy Prandtl number taken to be unity, and C the Smagorinsky constant. The diagonal term of τ_{ij} can be absorbed by a redefinition of the pressure. The resulting simulations are then technically called large eddy simulations (LES), though clearly the subgrid scale model terms become more prominent as the Rayleigh number increases. Even with inclusion of the extra subgrid scale terms, the numerical resolution available to us was unable to provide an accurate solution for $R = 10^7$. To test the sensitivity of our large eddy simulation results, computations were performed with $C = 0.15$ or 0.30. The horizontal velocity variance exhibited the largest variation, its value being approximately 40% larger for $C = 0.15$ than for $C = 0.3$ when $R = 10^6$. At this same Rayleigh number, the vertical velocity and scalar variance had a smaller variation of approximately 20% whereas the heat flux statistic showed almost no variation. The results we present will be for $C = 0.15$.

5. Numerical simulation results

The results from the DNS/LES computations for the mean temperature gradient and the second-moments for $R = 10^3$, 10^4, 10^5, 10^6 are shown in Figs. 1–6: the mean temperature gradient is presented in Fig. 1, the vertical and horizontal velocity variances and their sum are shown in Figs. 2–4, the temperature variance is shown in Fig. 5, and the heat flux is shown in Fig. 6.

The dashed line in Fig. 1 represents the temperature gradient $-\beta_0$ in the absence of fluid motion ($R < R_c$ – the laminar solution) whereas the solid lines represent the gradient at higher Rayleigh numbers. The mean temperature gradient converges towards zero with increasing Rayleigh number within a central well-mixed layer. The well-mixed layer is approximately the same length as the unstable layer $|x_2| < 1/\sqrt{3}$ of the laminar solution. Above and below the well-mixed layer are layers of partial mixing in which the temperature gradient converges at large Rayleigh numbers to a positive (stable) value less than the laminar value. Above and below these partially mixed layers, the mean temperature gradient eventually attains its laminar value. We thus distinguish three different layers in our turbulent flow as $R \to \infty$: a well-mixed layer with zero mean temperature gradient, partially

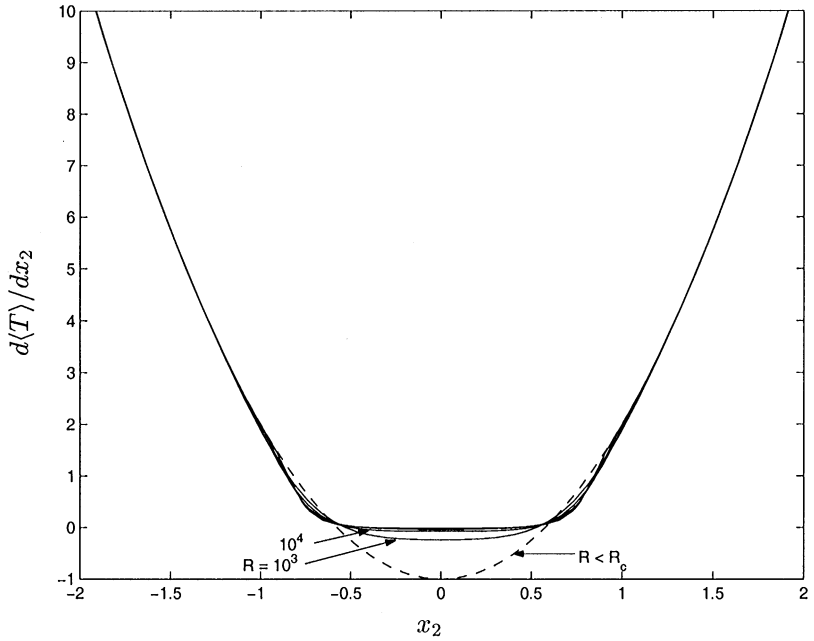

Fig. 1. The mean temperature gradient $\mathrm{d}\langle T\rangle/\mathrm{d}x_2$ versus vertical height x_2. The dashed line represents the laminar state ($R < R_c$) and the solid lines show the numerical simulation results for $R = 10^3,\ 10^4,\ 10^5,\ 10^6$.

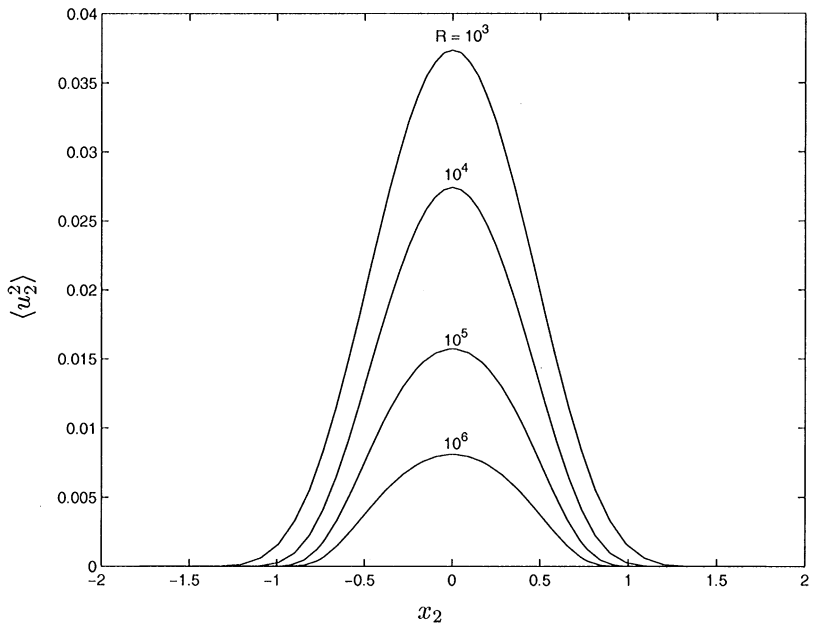

Fig. 2. The vertical velocity variance $\langle u_2^2\rangle$ versus vertical height x_2 from the numerical simulations for $R = 10^3,\ 10^4,\ 10^5,\ 10^6$.

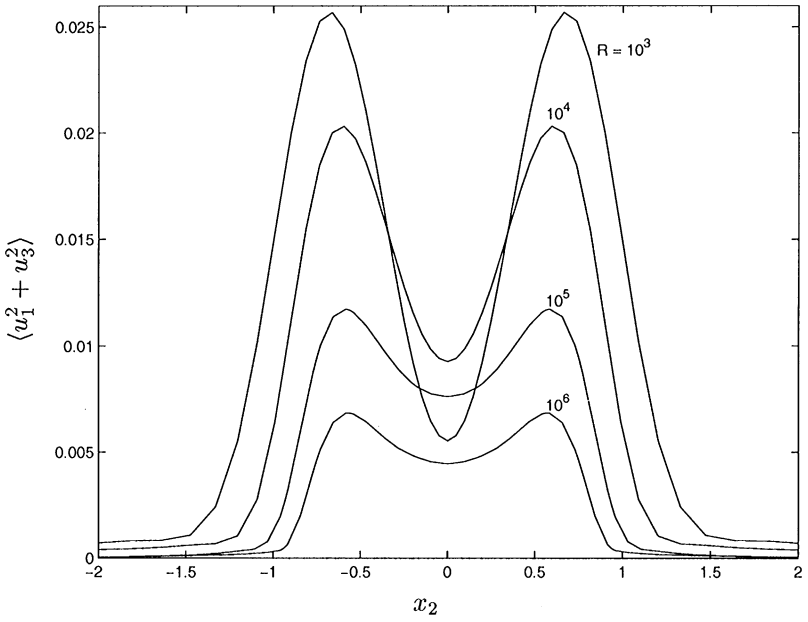

Fig. 3. The horizontal velocity variance $\langle u_1^2 + u_3^2 \rangle$ versus vertical height x_2 from the numerical simulations for $R = 10^3,\ 10^4,\ 10^5,\ 10^6$.

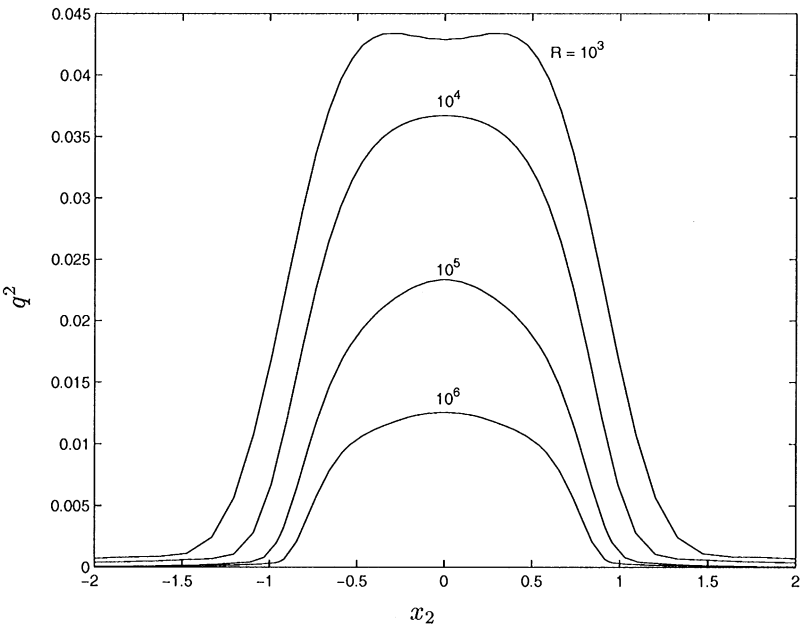

Fig. 4. The total velocity variance q^2 versus vertical height x_2 from the numerical simulations for $R = 10^3,\ 10^4,\ 10^5,\ 10^6$.

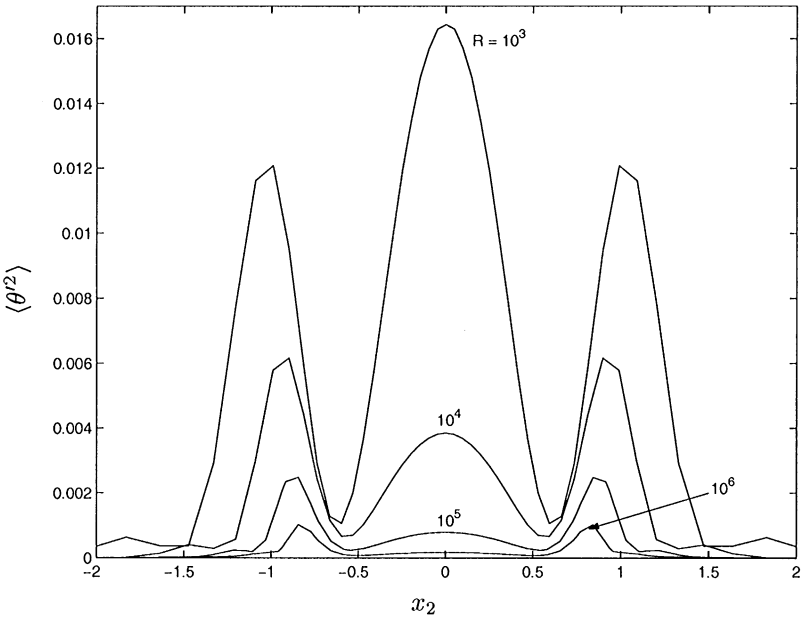

Fig. 5. The temperature variance $\langle\theta'^2\rangle$ versus vertical height x_2 from the numerical simulations for $R=10^3,\ 10^4,\ 10^5,\ 10^6$.

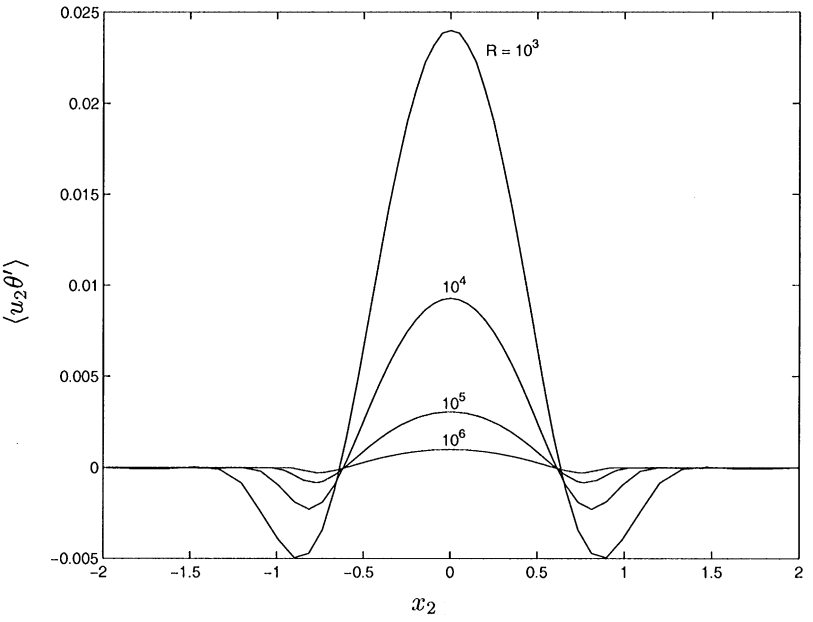

Fig. 6. The heat flux $\langle u_2\theta'\rangle$ versus vertical height x_2 from the numerical simulations for $R=10^3,\ 10^4,\ 10^5,\ 10^6$.

mixed layers above and below the well-mixed layer, and unmixed layers far above and below the partially mixed layers.

In Fig. 2, the vertical velocity variance is observed to attain its maximum in the center of the well-mixed layer whereas in Fig. 3, the horizontal velocity variance is observed to be maximum within the partially mixed layers. Both (nondimensional) velocity variances decrease with increasing Rayleigh numbers. The outer maxima of the horizontal velocity variances signifies a turning of the fluid velocity from a primarily vertical to a horizontal direction, similar to that which occurs when a fluid encounters a solid wall. The total velocity variance is shown in Fig. 4. At large Rayleigh numbers, there is only a single maximum in the center of the well-mixed layer; however the region over which the total velocity variance is appreciable is noticeably broader than that for the vertical variance alone.

The temperature variance, shown in Fig. 5, has local maxima both in the center of the well-mixed layer and within the upper and lower partially mixed layers. Both maxima decrease with increasing Rayleigh number. Although the maximum is largest in the well-mixed layer at the lowest Rayleigh number, the maxima within the partially mixed layers become largest at higher Rayleigh numbers. The experimental observation of a large temperature variance within the stable fluid layers in penetrative convection was first reported by Townsend (1964) based on his ice-water experiments and was attributed to the excitation of internal gravity waves.

The heat flux, shown in Fig. 6, is positive within the well-mixed layer with maximum in the center, and negative within the partially mixed layers. The heat flux is related to the mean temperature gradient via Eq. (26), and the change in sign of the heat flux coincides approximately with the change in sign of $\beta_0(x_2)$. The usual physical interpretation is that the turbulent motions act to mix the mean temperature gradient created by the internal heat source.

Finally, in Fig. 7 we plot the temperature increment θ_∞, (19), of the fluid in the unmixed layers versus the Rayleigh number R. It is observed that θ_∞ slowly increases with R, though it is impossible to conclude from the data whether this increase continues indefinitely or whether θ_∞ eventually approaches a constant value as $R \to \infty$. In Section 6 we will argue for the latter conclusion using results from an analytical model.

6. Analytic scaling laws from a turbulence model

6.1. Second-moment closure

In the second-moment equations (21)–(26), only the source/sink terms represented by IV are in terms of the second-moments. Closure assumptions must be made for the terms I–III if these equations are to be solved directly. In this section, we show how some widely used and relatively simple closure models enable us to predict the high Rayleigh number scaling of the simulation statistics.

Models at the level of the second-moment equations have been developed for stratified turbulence (see, for instance, Mellor and Yamada, 1982; Launder, 1989; Craft et al., 1996). We consider directly the second-moment equations for q^2, $\langle\theta'^2\rangle$ and $\langle u_2\theta'\rangle$. We assume a statistically steady state so that the second-moments are functions only of the vertical coordinate x_2. Modelling the moment equation for q^2 instead of separately modelling the equations for the vertical and horizontal velocity variances

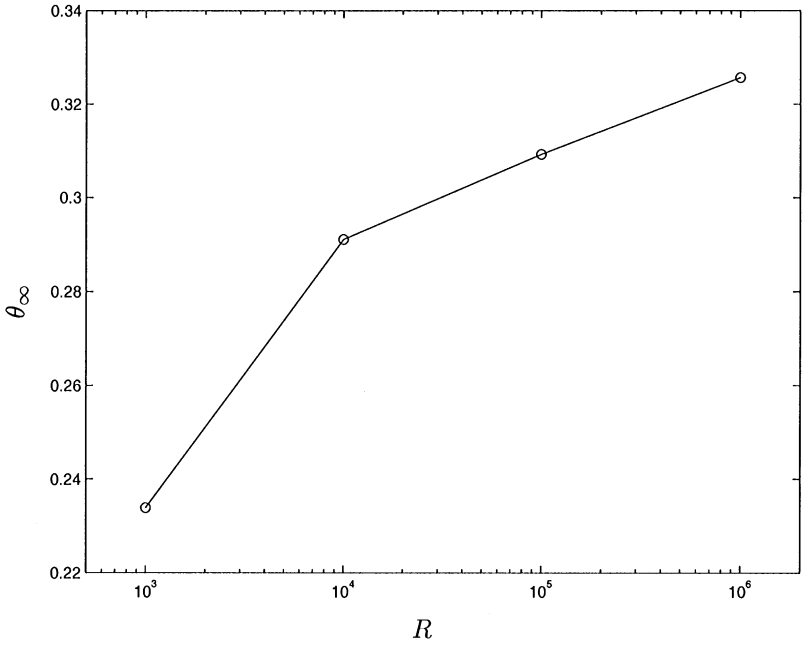

Fig. 7. Computation of θ_∞, defined in Eq. (19), versus R from the numerical simulation data.

alleviates the need for treatment of the difficult to model pressure-strain term. The pressure-strain term is responsible for the generation of the horizontal velocity variance – there being no other source term in this equation – and is usually modelled with a return-to-isotropy assumption (Launder, 1989). However, within the partially mixed fluid layers the numerical simulation results show that the horizontal variance becomes larger than the vertical variance so that a return-to-isotropy type of model would not be able to reproduce this wall-like effect.

The dissipation terms I are modelled using a Kolmogorov-like argument and local isotropy assumption as

$$\mathrm{I}_{q^2} = -\frac{2q^3}{\Lambda_1}, \quad \mathrm{I}_{\langle\theta'^2\rangle} = -\frac{2q}{\Lambda_2}\langle\theta'^2\rangle, \quad \mathrm{I}_{\langle u_2\theta'\rangle} = 0, \tag{33}$$

where Λ_1 and Λ_2 are nondimensional length scales. The transport terms are modelled as

$$\mathrm{II}_{q^2} = \frac{\mathrm{d}}{\mathrm{d}x_2}\left(L_1 q \frac{\mathrm{d}}{\mathrm{d}x_2} q^2\right), \quad \mathrm{II}_{\langle\theta'^2\rangle} = \frac{\mathrm{d}}{\mathrm{d}x_2}\left(L_2 q \frac{\mathrm{d}}{\mathrm{d}x_2}\langle\theta'^2\rangle\right),$$

$$\mathrm{II}_{\langle u_2\theta'\rangle} = \frac{\mathrm{d}}{\mathrm{d}x_2}\left(L_3 q \frac{\mathrm{d}}{\mathrm{d}x_2}\langle u_2\theta'\rangle\right), \tag{34}$$

where L_1, L_2, and L_3 are additional nondimensional length scales. Finally, the temperature–pressure gradient term is modelled as

$$\mathrm{III}_{\langle u_2\theta'\rangle} = -\frac{q}{\lambda}\langle u_2\theta'\rangle + (\zeta - 1)\langle\theta'^2\rangle, \tag{35}$$

where λ is another nondimensional length scale and ζ is a constant between zero and unity. The first term in the model of the temperature–pressure gradient plays a role analogous to the dissipation terms I. The second term is omitted by Mellor and Yamada (1982), but is included by Launder (1989). It serves to modify the coefficient of the term $\langle\theta'^2\rangle$ in the source $\mathrm{IV}_{\langle u_2\theta'\rangle}$ from unity to ζ. Finally, since $\langle u_2^2\rangle$ appears explicitly in $\mathrm{IV}_{\langle u_2\theta'\rangle}$, this term must now be modelled and we make the convenient (though erroneous) assumption that

$$\langle u_2^2\rangle = \gamma q^2 \tag{36}$$

with γ a constant between zero and unity.

In general, the nondimensional length scales Λ_1, Λ_2, L_1, L_2, L_3 and λ depend on the vertical coordinate x_2. Mellor and Yamada (1982) set them all proportional and formulate an additional length scale equation. Launder (1989) eliminates these length scales (again all proportional) in favor of the energy dissipation rate $\varepsilon = -I_{q^2}/2$ and formulates an additional evolution equation for ε. Since the characteristic energy containing length scale of our problem is set by the internal heat source by way of β_0, it is plausible that this master length scale will be independent of Rayleigh number at asymptotically large values. Furthermore, an analytical solution of the above model (with some additional simplifications) is possible if we assume that all the length scales are independent of x_2. Although this may result in a quantitatively inaccurate model, we hope that the solution will be qualitatively correct. Also, we then have the distinct advantage of explicitly obtaining the analytical high Rayleigh number scaling of the moments.

6.2. An analytical model without penetration

We begin by considering a simpler set of model equations obtained by neglecting transport, i.e., taking $L_1 = L_2 = L_3 = 0$. The physical role of the transport terms is to move the turbulent fluctuations generated in the unstable middle layer to the stable upper and lower layers, and without these terms it is expected that the solution will have zero variances within the stable layers. With the above simplification, the closed model equations for the statistics q^2, $\langle\theta'^2\rangle$, $\langle u_2\theta'\rangle$ and $\mathrm{d}\langle T\rangle/\mathrm{d}x_2$ become

$$\frac{q^3}{\Lambda_1} = \langle u_2\theta'\rangle, \tag{37}$$

$$\frac{q}{\Lambda_2}\langle\theta'^2\rangle = -\langle u_2\theta'\rangle\frac{\mathrm{d}\langle T\rangle}{\mathrm{d}x_2}, \tag{38}$$

$$\frac{q}{\lambda}\langle u_2\theta'\rangle = \zeta\langle\theta'^2\rangle - \gamma q^2\frac{\mathrm{d}\langle T\rangle}{\mathrm{d}x_2}, \tag{39}$$

$$\frac{\mathrm{d}\langle T\rangle}{\mathrm{d}x_2} = (\sigma R)^{1/2}\langle u_2\theta'\rangle - \beta_0. \tag{40}$$

After some algebraic manipulation, we find that the solution of Eqs. (37)–(40) for the mean temperature gradient is either explicitly given by

$$\frac{\mathrm{d}\langle T\rangle}{\mathrm{d}x_2} = -\beta_0 \tag{41}$$

or implicitly given by

$$\frac{\mathrm{d}\langle T\rangle}{\mathrm{d}x_2} = -\left(\gamma + \frac{\zeta\Lambda_2}{\Lambda_1}\right)^{-1} \Lambda_1^{-1/3}\lambda^{-1}\beta_0^{2/3}(\sigma R)^{-1/3}\left(1 + \frac{1}{\beta_0}\frac{\mathrm{d}\langle T\rangle}{\mathrm{d}x_2}\right)^{2/3} \tag{42}$$

the former solution applicable to the upper and lower unmixed layers and the latter to the central well-mixed layer. For high Rayleigh numbers in the well-mixed layer

$$\left|\frac{1}{\beta_0}\frac{\mathrm{d}\langle T\rangle}{\mathrm{d}x_2}\right| \ll 1 \tag{43}$$

so that to leading-order in σR,

$$\frac{\mathrm{d}\langle T\rangle}{\mathrm{d}x_2} = -\left(\gamma + \frac{\zeta\Lambda_2}{\Lambda_1}\right)^{-1} \Lambda_1^{-1/3}\lambda^{-1}\beta_0^{2/3}(\sigma R)^{-1/3}, \tag{44}$$

$$q^2 = \Lambda_1^{2/3}\beta_0^{2/3}(\sigma R)^{-1/3}, \tag{45}$$

$$\langle\theta'^2\rangle = \Lambda_1^{-2/3}\Lambda_2\lambda^{-1}\left(\gamma + \frac{\zeta\Lambda_2}{\Lambda_1}\right)^{-1} \beta_0^{4/3}(\sigma R)^{-2/3}, \tag{46}$$

$$\langle u_2\theta'\rangle = \beta_0(\sigma R)^{-1/2}. \tag{47}$$

These statistics in the central well-mixed layer match (when $\beta_0 = 0$ at $x_2 = \pm 1/\sqrt{3}$) with their laminar form in the upper and lower unmixed layers,

$$\frac{\mathrm{d}\langle T\rangle}{\mathrm{d}x_2} = -\beta_0, \quad q^2 = 0, \quad \langle\theta'^2\rangle = 0, \quad \langle u_2\theta'\rangle = 0 \tag{48}$$

as a result of the lack of transport within this model.

We have thus obtained within our simplified turbulence model the large Rayleigh number scalings of the moments in the central well-mixed layer. The decrease in the velocity and temperature variance in the well-mixed layer with increasing Rayleigh number and the approach of the temperature gradient to zero is in qualitative agreement with our numerical simulation results, and a more quantitative comparison will be made in Section 7. We note that our obtained scalings for the velocity variance agree with those found earlier by Zahn et al. (1982) for hexagonal cells and not for those obtained by them using rolls. (To compare our result (45) to that of Zahn et al., Eq. (15) must be used to convert units.)

Although the velocity variance decreases with Rayleigh number as $R^{-1/3}$, the Reynolds number Re of the flow field, defined in Eq. (17) with the velocity scale U taken to be proportional to q at $x_2 = 0$, increases with Rayleigh number as $Re \sim R^{1/3}$ so that the fluid motion is more turbulent with increasing Rayleigh number in the usual sense.

Our analytic results also demonstrate the importance of each of the modelled terms through the nondimensional length scales Λ_1, Λ_2 and λ, and the constants γ and ζ. For instance, the solution diverges in the absence of viscous dissipation ($\Lambda_1 \to \infty$) but remains finite in the absence of thermal conduction ($\Lambda_2 \to \infty$). Also, the first of the temperature–pressure gradient terms (which goes to zero as $\lambda \to \infty$) is necessary for the creation of nonzero temperature variance within the central well-mixed layer.

6.3. An analytical model with penetration

The above simplified model excludes the physics of penetration. To include this effect we need to consider nonzero transport. The transport terms in the temperature variance and heat flux equations are difficult to treat analytically; however, the term in the energy equation is simpler to consider since for constant L_1,

$$\mathrm{II}_{q^2} = \frac{\mathrm{d}}{\mathrm{d}x_2}\left(L_1 q \frac{\mathrm{d}}{\mathrm{d}x_2} q^2\right) = \frac{2}{3} L_1 \frac{\mathrm{d}^2}{\mathrm{d}x_2^2} q^3. \tag{49}$$

To consider some aspect of transport analytically, we thus take $L_2 = L_3 = 0$, and $L_1 \neq 0$. Our model equations now become

$$\frac{L_1}{3}\frac{\mathrm{d}^2}{\mathrm{d}x_2^2} q^3 - \frac{1}{\Lambda_1} q^3 = -\langle u_2 \theta' \rangle, \tag{50}$$

$$\frac{q}{\Lambda_2}\langle \theta'^2 \rangle = -\langle u_2 \theta' \rangle \frac{\mathrm{d}\langle T \rangle}{\mathrm{d}x_2}, \tag{51}$$

$$\frac{q}{\lambda}\langle u_2 \theta' \rangle = \zeta \langle \theta'^2 \rangle - \gamma q^2 \frac{\mathrm{d}\langle T \rangle}{\mathrm{d}x_2}, \tag{52}$$

$$\frac{\mathrm{d}\langle T \rangle}{\mathrm{d}x_2} = (\sigma R)^{1/2} \langle u_2 \theta' \rangle - \beta_0. \tag{53}$$

From Eqs. (51)–(53), we can derive a quadratic equation for $\mathrm{d}\langle T \rangle / \mathrm{d}x_2$ in terms of q:

$$\left(\frac{\mathrm{d}\langle T \rangle}{\mathrm{d}x_2}\right)^2 + \left(\beta_0 + \frac{q^2}{\zeta \Lambda_2 \lambda} + \frac{\gamma(\sigma R)^{1/2}}{\zeta \Lambda_2} q^3\right)\left(\frac{\mathrm{d}\langle T \rangle}{\mathrm{d}x_2}\right) + \frac{q^2}{\zeta \Lambda_2 \lambda}\beta_0 = 0. \tag{54}$$

To solve the remaining Eq. (50), we need to determine the heat flux $\langle u_2 \theta' \rangle$ using Eqs. (54) and (53), i.e.,

$$\langle u_2 \theta' \rangle = (\sigma R)^{-1/2}\left(\beta_0 + \frac{\mathrm{d}\langle T \rangle}{\mathrm{d}x_2}\right). \tag{55}$$

We consider the large Rayleigh number asymptotics. Within the well-mixed layer, the mean temperature gradient approaches zero as $R \to \infty$ so that the β_0 term of Eq. (55) dominates over the mean temperature gradient. Above and below the well-mixed layer the mean temperature gradient approaches a nonzero value, and since $q \to 0$ as $R \to \infty$, Eq. (54) simplifies to

$$\left(\frac{\mathrm{d}\langle T \rangle}{\mathrm{d}x_2}\right) + \left(\beta_0 + \frac{\gamma(\sigma R)^{1/2}}{\zeta \Lambda_2} q^3\right) = 0. \tag{56}$$

The asymptotic high Rayleigh number solution for the heat flux is thus given by

$$\langle u_2 \theta' \rangle = \begin{cases} (\sigma R)^{-1/2}\beta_0 & \text{if } |x_2| < s/2, \\ -\gamma(\zeta \Lambda_2)^{-1} q^3 & \text{if } |x_2| > s/2, \end{cases} \tag{57}$$

where s is the height of the well-mixed layer. The precise value of s is to be determined after a solution for q is found by requiring the continuity of the heat flux at $\pm s/2$. We comment that the heat flux given by Eq. (57) agrees qualitatively with the simulation results shown in Fig. 6, being positive in the central well-mixed layer and negative in the upper and lower partially mixed layers.

We are thus left with solving a linear second-order differential equation for q^3. We define the parameters

$$c = \frac{3}{L_1}, \quad a^2 = \frac{c}{\Lambda_1}, \quad b^2 = a^2\left(1 + \frac{\gamma\Lambda_1}{\zeta\Lambda_2}\right). \tag{58}$$

Then the differential equation for q^3 becomes

$$\frac{\mathrm{d}^2}{\mathrm{d}x_2^2}q^3 - a^2 q^3 = -c(\sigma R)^{-1/2}\beta_0, \quad |x_2| < s/2, \tag{59}$$

$$\frac{\mathrm{d}^2}{\mathrm{d}x_2^2}q^3 - b^2 q^3 = 0, \quad |x_2| > s/2 \tag{60}$$

with the boundary conditions $q^3 \to 0$ at $x_2 = \pm\infty$, and continuity of q^3 and its derivative at $x_2 = \pm s/2$. Using $\beta_0 = 1 - 3x_2^2$, the solution is

$$q^3(\sigma R)^{1/2} = \begin{cases} A\exp[b(x_2 + s/2)] & \text{if } x_2 < -s/2, \\ B[\exp(ax_2) + \exp(-ax_2)] + ca^{-2}(1 - 6a^{-2} - 3x_2^2) & \text{if } |x_2| < s/2, \\ A\exp[-b(x_2 - s/2)] & \text{if } x_2 > s/2, \end{cases} \tag{61}$$

where the coefficients A and B are functions of a, b, c and s but are independent of σR. The exact result for the coefficients is not particularly illuminating and we omit it here; rather we observe that $q^2 \propto (\sigma R)^{-1/3}$, and from Eq. (57), $\langle u_2\theta'\rangle \propto (\sigma R)^{-1/2}$ over the entire domain. Using Eq. (54), we also find that in the well-mixed layer $\mathrm{d}\langle T\rangle/\mathrm{d}x_2 \propto (\sigma R)^{-1/3}$ whereas it scales like $(\sigma R)^0$ above and below this layer.

The scaling of the temperature variance $\langle\theta'^2\rangle$ may now be determined from Eq. (51), i.e.

$$\langle\theta'^2\rangle = -\Lambda_2\langle u_2\theta'\rangle q^{-1}\frac{\mathrm{d}\langle T\rangle}{\mathrm{d}x_2}. \tag{62}$$

As a consequence of the different scaling of the mean temperature gradient, in the well-mixed layer $\langle\theta'^2\rangle \propto (\sigma R)^{-2/3}$ whereas above and below this layer $\langle\theta'^2\rangle \propto (\sigma R)^{-1/3}$. Hence for large Rayleigh numbers the temperature variance in the central well-mixed layer is small compared to that in the partially mixed layers above and below. This is in qualitative agreement with the results of our numerical simulations, and with the ice-water experiments of Townsend (1964).

It is easily seen that inclusion of the transport terms in the temperature variance and heat flux equations will not modify the above scaling laws.

The height of the well-mixed layer s can be determined from continuity of the heat flux and the analytical solution for the coefficient A (which depends on s). This leads to a transcendental equation for s which depends on all the parameters of the second-moment closure model. Rather than pursue this further here, it is more illuminating to consider a simpler physical model.

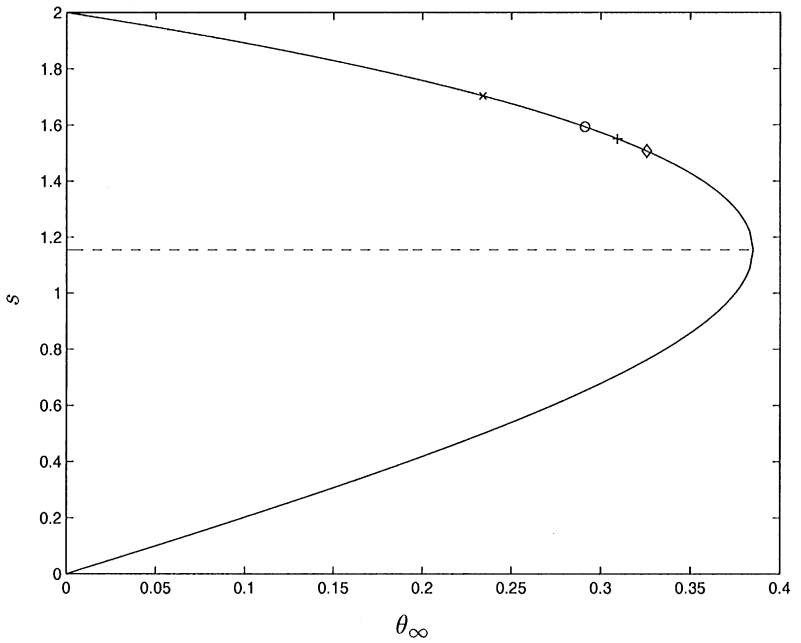

Fig. 8. The solid line is the height s of the well-mixed layer versus θ_∞, obtained by solving the cubic equation given in Eq. (64). The dashed line at $s=2/\sqrt{3}$ corresponds to the height of the (laminar) unstable layer. The symbols on the plot correspond to values of θ_∞ obtained from the numerical simulations: ($\times$) $R=10^3$; ($\circ$) $R=10^4$; ($+$) $R=10^5$; ($\diamond$) $R=10^6$.

6.4. A model for the penetration length

We consider $R \to \infty$ and assume only mixed and unmixed layers, i.e., we take the mean temperature gradient to be zero over a layer of height s, and to be the same as the laminar temperature gradient above and below this layer. A similar physical model was also proposed by Zahn et al. (1982). Now, the mean temperature distribution itself is shifted above and below the mixed layer by the constant θ_∞, and from Eq. (19) and the scaling of the heat flux derived in Section 6.3, θ_∞ approaches a constant finite value as $R \to \infty$. The temperature distribution at high Rayleigh numbers thus takes the modelled form

$$T(x_2) = \begin{cases} T_0(x_2) - \theta_\infty & \text{if } x_2 < -s/2, \\ 0 & \text{if } -s/2 < x_2 < s/2, \\ T_0(x_2) + \theta_\infty & \text{if } x_2 > s/2. \end{cases} \tag{63}$$

Continuity of the modelled temperature distribution at $x_2 = \pm s/2$, and use of the nondimensional Matthews' form $T_0 = x_2^3 - x_2$ results in the following cubic equation for s:

$$\left(\frac{s}{2}\right)^3 - \left(\frac{s}{2}\right) + \theta_\infty = 0. \tag{64}$$

A graph of the real positive solutions of Eq. (64) for s as a function of θ_∞ is given by the solid line in Fig. 8. The unstable layer of the laminar fluid has height $2/\sqrt{3}$ (represented by the dashed-line),

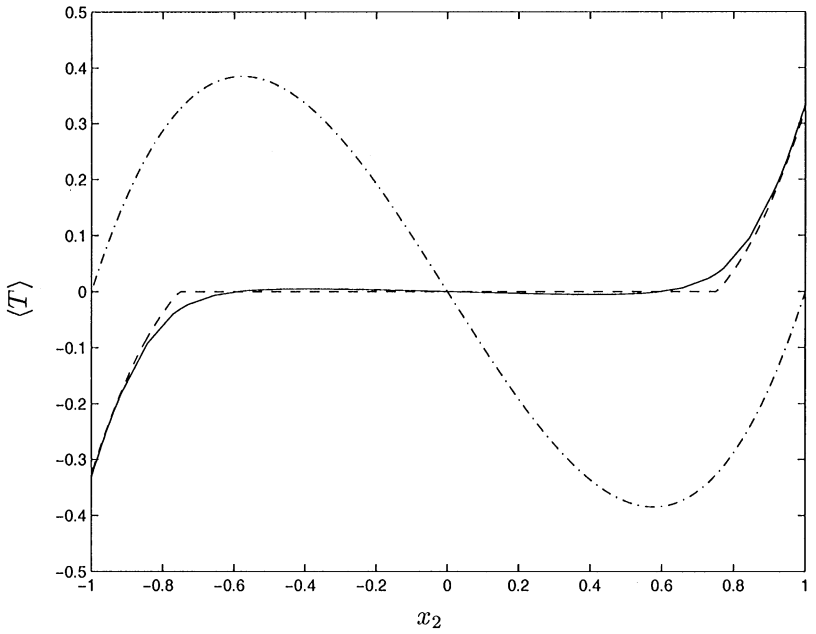

Fig. 9. Comparison of $\langle T \rangle$ from the numerical simulation data with $R = 10^6$ (solid line) and the two layer model profile (dashed line) with $\theta_\infty = 0.326$. Also for comparison we plot $T_0(x_2)$ (dashed-dot line).

obtained from Eq. (13) by solving $\beta_0(x_2) = 0$, and the curve lying above the dashed line corresponds to complete mixing of part of the stable temperature gradient. The solution curve lying below the dashed line corresponds to an incomplete mixing of the unstable temperature gradient and is discarded on physical grounds. Also shown as points on the curve are the results for θ_∞ from the numerical simulations, previously presented in Fig. 7.

There are two interesting limits. First, maximum penetration occurs for $s = 2$ corresponding to $\theta_\infty = 0$. From Eq. (28), this solution thus has vanishing turbulent dissipation rate (as $R \to \infty$) and all of the turbulence energy created in the central layer is eliminated above and below by work done against the buoyancy forces. Second, no penetration occurs when $s = 2/\sqrt{3} \approx 1.155$, and from Eq. (64) this occurs when $\theta_\infty = 2\sqrt{3}/9 \approx 0.3849$. Within the model, this is the largest value attainable by θ_∞ (and is in fact the value obtainable in Section 6.2 from the solution of the second-moment model without penetration). In this second limiting case, all of the turbulence energy generated in the central layer is dissipated by viscosity within this layer.

The above model is simplistic in that we approximate the true temperature profile consisting of well-mixed, partially mixed, and unmixed layers by two layers. Nevertheless, it is of interest to compare the model and actual temperature profiles. The temperature profile obtained from the numerical simulation for $R = 10^6$ (solid line) and the approximate two-layer model profile (dashed line) taking $\theta_\infty = 0.326$ are shown in Fig. 9. For comparison purposes, the laminar temperature profile T_0 is also shown (dashed-dot line). The two-layer model is observed to approximate reasonably the actual temperature profile.

Fig. 9 suggests a definition for a penetration distance using the two-layer model and Fig. 8. In Fig. 10, we plot the value of $\sqrt{3}s/2$ versus Rayleigh number obtained using the two-layer model

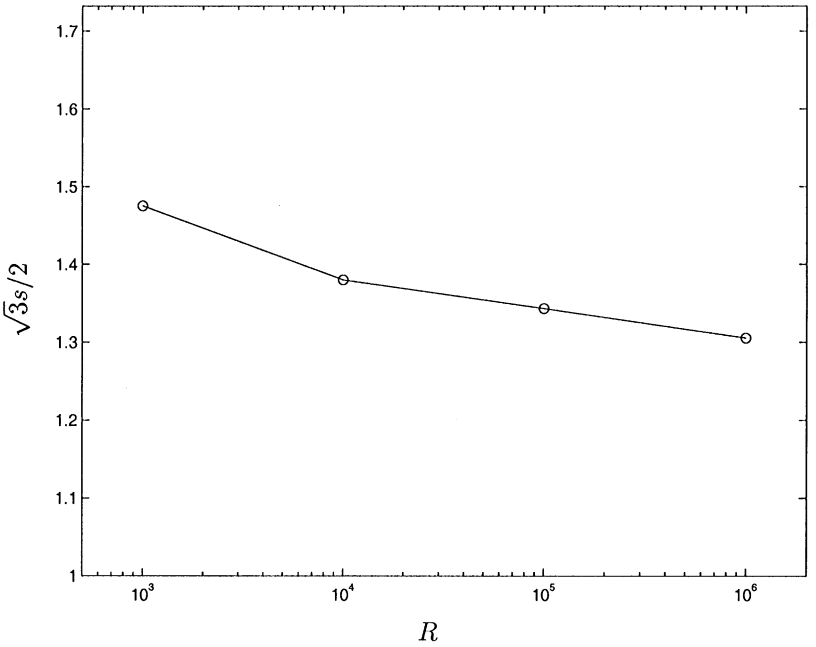

Fig. 10. Normalized height $\sqrt{3}s/2$ of the well-mixed layer versus Rayleigh number R, obtained from the two-layer model and the results of the numerical simulations.

and the values of θ_∞ from the numerical simulations. Within the two-layer model the ordinate may range from a maximum of $\sqrt{3}$ (corresponding to an approximate 36.6% extension of the (laminar) unstable layer on both sides) to a minimum of unity (corresponding to no extension) and we show this ordinate range in the figure. Evidently, the length of the well-mixed layer decreases with increasing Rayleigh number; however, the infinite Rayleigh number limit is unclear from the data. For $R = 10^6$, the height of the mixed layer is approximately 30% longer than the height of the (laminar) unstable layer, corresponding to a 15% extension above and below the unstable layer.

7. Scaling of the numerical simulation results

The Rayleigh number scalings of the statistics obtained in Section 6 are now compared to the results of the numerical simulations. A rescaling of the temperature variance is shown in Fig. 11a and b: $\langle\theta'^2\rangle$ is multiplied by $R^{2/3}$ and $R^{1/3}$, respectively. The former scaling is the theoretical result for the central well-mixed layer and the latter scaling is for the upper and lower partially mixed layers. Certainly, the different scaling of the temperature variance in the well-mixed and partially mixed layers is evident from these plots. Furthermore, the asymptotic analytical results seem to be reasonably well-obeyed considering the moderate Rayleigh numbers obtainable by the simulations.

In Fig. 12, the total velocity variance q^2 from the simulations is multiplied by $R^{1/3}$ and plotted versus vertical height x_2. This figure is to be compared to the unscaled plot given in Fig. 4. Although

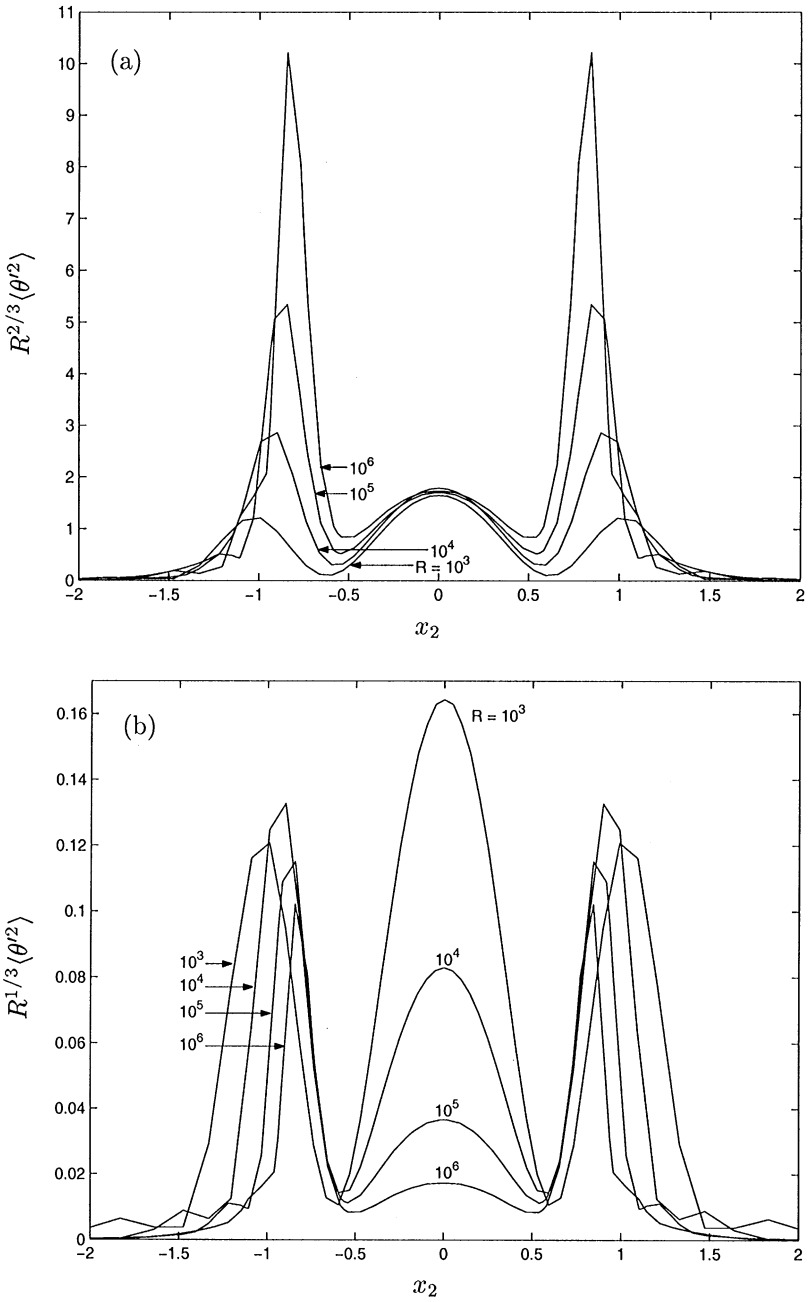

Fig. 11. The Rayleigh number scaled temperature variance $R^n\langle\theta'^2\rangle$ versus vertical height x_2 from the numerical simulations for $R = 10^3,\ 10^4,\ 10^5,\ 10^6$. (a) $n = \frac{2}{3}$ scaling appropriate for the central well-mixed layer; (b) $n = \frac{1}{3}$ scaling appropriate for the upper and lower partially mixed layers.

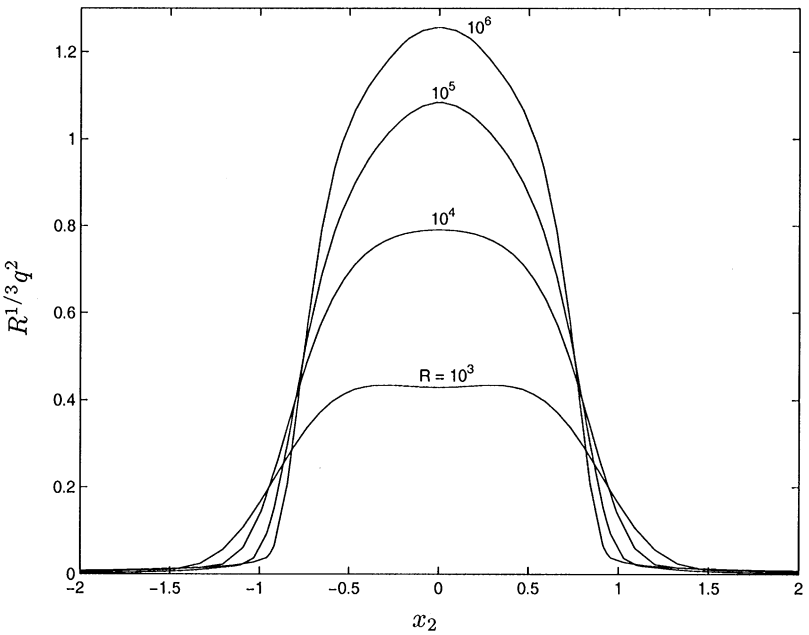

Fig. 12. The Rayleigh number scaled total velocity variance $R^{1/3}q^2$ versus vertical height x_2 from the numerical simulations for $R = 10^3,\ 10^4,\ 10^5,\ 10^6$.

a tendency towards scaling is observed in Fig. 12, it seems that a definitive test of the high Rayleigh number scaling law obtained in Section 6 is unattainable at these moderate Rayleigh numbers.

Finally, in Fig. 13 the heat flux $\langle u_2\theta'\rangle$ is multiplied by $R^{1/2}$ and plotted versus x_2 for the various Rayleigh numbers simulated. At the highest Rayleigh numbers, the asymptotic analytic scaling laws seem reasonably well-obeyed. In the well-mixed layer, the mean temperature gradient approaches zero with Rayleigh number so that from Eq. (55) the heat flux scales like $(\sigma R)^{-1/2}\beta_0$. In the center of the well-mixed layer $\beta_0 = 1$ so that the rescaled heat flux should be near unity and this is observed from the simulation for $R = 10^6$.

8. Summary

High Rayleigh number asymptotics for the velocity and scalar variances, heat flux, and mean temperature gradient were obtained from a simplified second-moment closure model and compared to results from direct and large eddy simulations. The computations attain Rayleigh numbers R four orders of magnitude above the critical value. Although this may be too low to decisively test the analytic scaling laws, qualitative agreement between the simulation results and the asymptotics provide us some confidence in their validity.

Of course our turbulence modelling is inexact and there remains the possibility that the scaling laws obtained from the model are incorrect. Nevertheless, the obtained scaling laws are insensitive to the precise details of the model (i.e., the model coefficients), but rather arise from the well-established

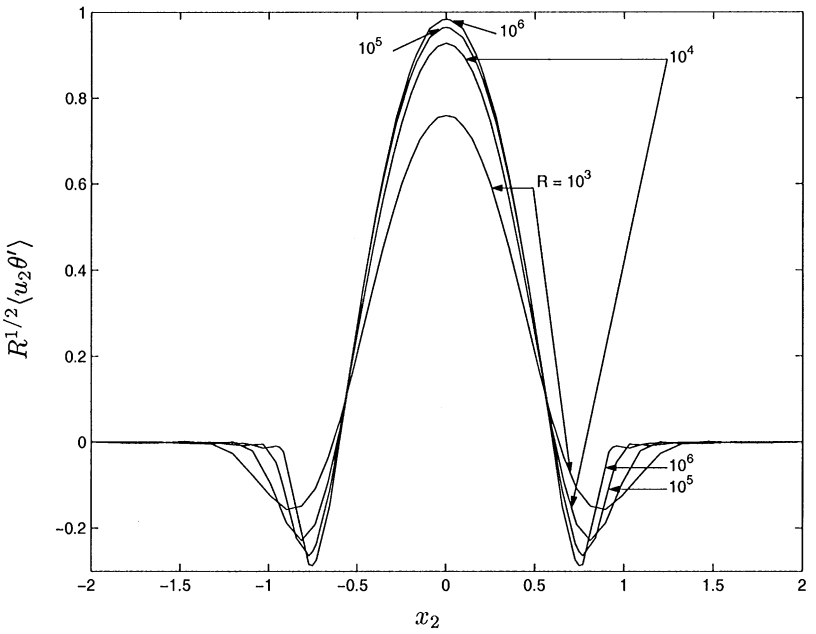

Fig. 13. The Rayleigh number scaled heat flux $R^{1/2}\langle u_2\theta'\rangle$ versus vertical height x_2 from the numerical simulations for $R = 10^3,\ 10^4,\ 10^5,\ 10^6$.

approximations that at high Reynolds numbers dissipation and transport are independent of the molecular coefficients of viscosity and diffusivity.

The computational results show three layers of mixing in the fluid: a central well-mixed layer of approximately the same extent as the (laminar) unstable layer in which the mean temperature gradient approaches zero as $R \to \infty$, partially mixed layers above and below the well-mixed layer in which the mean temperature gradient has reduced stability compared to its laminar value, and unmixed layers far above and below the partially mixed layers. An interesting result of the second-moment closure model – which finds some verification from the numerical simulations – is that the temperature variance scales differently on Rayleigh number in the well-mixed and partially mixed layers. As $R \to \infty$, the temperature variance in the partially mixed layer dominates by a factor of $R^{1/3}$. The second-moment closure model yields a simple explanation for this result: the temperature variance is proportional to the mean temperature gradient, and although the mean temperature gradient goes to zero as $R^{-1/3}$ in the well-mixed layer, it approaches a nonzero value in the partially mixed layers. Physically, temperature fluctuations are created by vertical fluid motion along a mean temperature gradient; the turbulent mixing reduces the mean temperature gradient to zero within the central well-mixed layer thus eliminating the source of temperature fluctuations.

Finally, upon approximating the three layers of mixing by a two-layer model we have been able to estimate the height of the mixed layer at $R = 10^6$ to be about 30% longer than the height of the (laminar) unstable layer (corresponding to approximately a 15% extension above and below). This 15% is to be compared to a 50% extension on both sides reported by Zahn et al. (1982) using a piece-wise linear temperature gradient with the unstable gradient of same magnitude as the stable

gradient. This difference in penetration may be due to the increased stability of our upper and lower layers because of our use of a quadratic temperature gradient. We also comment that our numerical simulations demonstrate a slow decrease in the penetration length with increasing Rayleigh number, though this is presumably a finite Rayleigh number effect.

Acknowledgements

J.R.C would like to thank Dr. V.M. Canuto for introducing him to the problem of penetrative convection. The computations presented here were performed on an Intel Paragon at The Hong Kong University of Science and Technology, and the support of the Centre for Computing Services and Telecommunications and the Hong Kong Research Grant Council is gratefully acknowledged.

References

Canuto, V.M., Christensen-Dalsgaard, J., 1998. Turbulence in astrophysics. Annu. Rev. Fluid Mech. 30, 167–198.

Craft, T.J., Ince, N.Z., Launder, B.E., 1996. Recent developments in second-moment closure for buoyancy-affected flows. Dyn. Atmos. Oceans 23, 99–114.

Gribov, V.N., Gurevich, L.E., 1957. On the theory of the stability of a layer located at a superadiabatic temperature gradient in a gravitational field. Sov. Phys. J.E.T.P. 4, 720–729.

Launder, B.E., 1989. The prediction of force field effects on turbulent shear flows via second-moment closure. In: Fernholz, H.-H., Fiedler, H.E. (Eds.), Advances in Turbulence, Vol. 2. Springer, Berlin.

Matthews, P.C., 1988. A model for the onset of penetrative convection. J. Fluid Mech. 188, 571–583.

Mellor, G.L., Yamada, T., 1982. Development of a turbulence closure model for geophysical fluid problems. Rev. Geophys. 20, 851–875.

Smagorinsky, J., 1963. General circulation experiments with the primitive equations. Mon. Weather Rev. 91, 99–164.

Spiegel, E.A., Veronis, G., 1960. On the Bousinesq approximation for a compressible fluid. Astrophys. J. 131, 442–447.

Straughan, B., 1993. Mathematical Aspects of Penetrative Convection. Longman Scientific and Technical, New York.

Townsend, A.A., 1964. Natural convection in water over an ice surface. Quart. J. Roy. Meteorol. Soc. 90, 248–259.

Tse, K.L., 2000. Simulation of convection problem with adaptive spectral domain decomposition method. Appl. Numer. Math. 33, 267–274.

Tse, K.L., Chasnov, J.R., 1998. A Fourier-Hermite pseudospectral method for penetrative convection. J. Comput. Phys. 142, 489–505.

Zahn, J.-P., Toomre, J., Latour, J., 1982. Nonlinear modal analysis of penetrative convection. Geophys. Astrophys. Fluid Dyn. 22, 159–193.